SPACE SCIENCES

Fusible mantle cumulates trigger young mare volcanism on the cooling Moon

Bin Su[1]†*, Jiangyan Yuan[1]†, Yi Chen[1]*, Wei Yang[2], Ross N. Mitchell[1], Hejiu Hui[3,4], Hao Wang[1], Hengci Tian[2], Xian-Hua Li[1], Fu-Yuan Wu[1]

The Chang'E-5 (CE5) mission has demonstrated that lunar volcanism was still active until two billion years ago, much younger than the previous isotopically dated lunar basalts. How the small Moon retained enough heat to drive such late volcanism is unknown, particularly as the CE5 mantle source was anhydrous and depleted in heat-producing elements. We conduct fractional crystallization and mantle melting simulations that show that mantle melting point depression by the presence of fusible, easily melted components could trigger young volcanism. Enriched in calcium oxide and titanium dioxide compared to older Apollo magmas, the young CE5 magma was, thus, sourced from the overturn of the late-stage fusible cumulates of the lunar magma ocean. Mantle melting point depression is the first mechanism to account for young volcanism on the Moon that is consistent with the newly returned CE5 basalts.

INTRODUCTION

As observed from Earth, the Moon is two-toned, with the bright anorthositic highlands and the dark basaltic maria. The former were formed by plagioclase flotation in the lunar magma ocean (LMO) (*1*, *2*), and the latter are considered to have formed by the remelting of the LMO cumulate mantle (*3*, *4*). Although mare basalts make up <1% by volume of the lunar crust, they provide essential information for the origin and evolution of the lunar interior (*4*, *5*). For instance, the compositions of mare basalts are influenced by melting temperature and pressure conditions, serving as probes into the Moon's thermal state (*6*, *7*). Mare basalts returned by the Apollo and Luna missions indicated that lunar volcanism was concentrated between ca. 3.8 and 3.1 billion years (Ga) ago (*8*), with the youngest dated volcanism at 2.9 to 2.8 Ga ago (*9*). The new mare basalt samples returned by the Chang'E-5 (CE5) mission, however, extend the eruption ages of lunar volcanism to ca. 2.0 Ga ago (*10*, *11*). This notable finding thus raises the question of how the young volcanism was generated on the cooling Moon. Furthermore, its eruption was related neither to radiogenic heating (*10*–*12*) nor to hydrous melting (*13*), compelling the consideration of other mechanisms.

To address this issue, one should first ascertain the source materials and melting conditions of the CE5 basalts. The lunar mantle is thought to be compositionally heterogeneous (*14*, *15*) and has not yet been sampled. Therefore, it is difficult to forward model lunar mantle melting. In addition, most mare basalts have undergone fractional crystallization during eruption, making their compositions deviate to different degrees from those of their primary magmas (*4*, *6*). Hence, unraveling the fractional crystallization processes to define primary magma compositions becomes the key to understanding mare basalt petrogenesis. The ancient Apollo basalts are proposed to have undergone <~30% olivine-dominated fractionation (*6*, *16*), whereas the young CE5 basalts underwent more extensive (43 to 78%) fractional crystallization (*12*). Whether these different eras of mare volcanism had a similar primary magma or originated from distinct sources or depths reflecting the Moon's thermal evolution is unknown. Distinguishing the petrogenesis of mare basalts over time can help decode the cause of the young lunar volcanic activity.

RESULTS AND DISCUSSION

This study selected 27 representative basalt clasts in the CE5 soil samples for bulk rock major element analyses. All clasts have particle sizes of >500 μm so as to contain abundant mineral grains in each clast. These clasts consist mainly of clinopyroxene, plagioclase, ilmenite, and olivine, with minor Cr-spinel, troilite, and mesostasis (fig. S1) (*17*). As compositional zoning in olivine and clinopyroxene is ubiquitous (*12*), bulk major element compositions of these clasts were measured using scanning electron microscopy and energy-dispersive x-ray spectroscopy quantitative mapping techniques (see Materials and Methods) (*18*). Our analytical results show that the CE5 basalts mostly have <6 weight % (wt %) of TiO_2 (average of 5.5 wt %; table S1) and can be classified as low-Ti type (*3*). The low-Ti classification is further supported by titanium in olivine (*19*) and the appearance of tabular to lamellar ilmenite cross-cutting the early olivine and clinopyroxene (fig. S2), which differ from the Apollo high-Ti basalts (*6*, *16*). The mineral compositions, isotopic chemistry, and geochronology together reveal that the CE5 basalt clasts most likely originated from a single lava flow (*11*, *12*). To synthetically evaluate the fractional crystallization processes of the old (ca. 3.8 to 3.1 Ga ago) volcanism, all Apollo basalt data used here are non-site specific and are analyzed using kernel density estimation (Fig. 1). This estimation can diminish the influence of magmatic assimilation and highlight the degree of fractional crystallization. Compared with Apollo samples (*20*–*22*), the most prominent feature of CE5 basalts is the relatively low MgO contents (Fig. 1), matching with their lower Mg# [Mg/(Mg + Fe)] of olivine and clinopyroxene (*12*, *17*). In the following sections, we conduct a series of modeling simulations—fractional crystallization,

[1]State Key Laboratory of Lithospheric Evolution, Institute of Geology and Geophysics, Chinese Academy of Sciences, Beijing 100029, China. [2]Key Laboratory of Earth and Planetary Physics, Institute of Geology and Geophysics, Chinese Academy of Sciences, Beijing 100029, China. [3]State Key Laboratory of Mineral Deposits Research and Lunar and Planetary Science Institute, School of Earth Sciences and Engineering, Nanjing University, Nanjing 210023, China. [4]CAS Center for Excellence in Comparative Planetology, Hefei 230026, China.
*Corresponding author. subin@mail.iggcas.ac.cn (B.S.); chenyi@mail.iggcas.ac.cn (Y.C.)
†These authors contributed equally to this work.

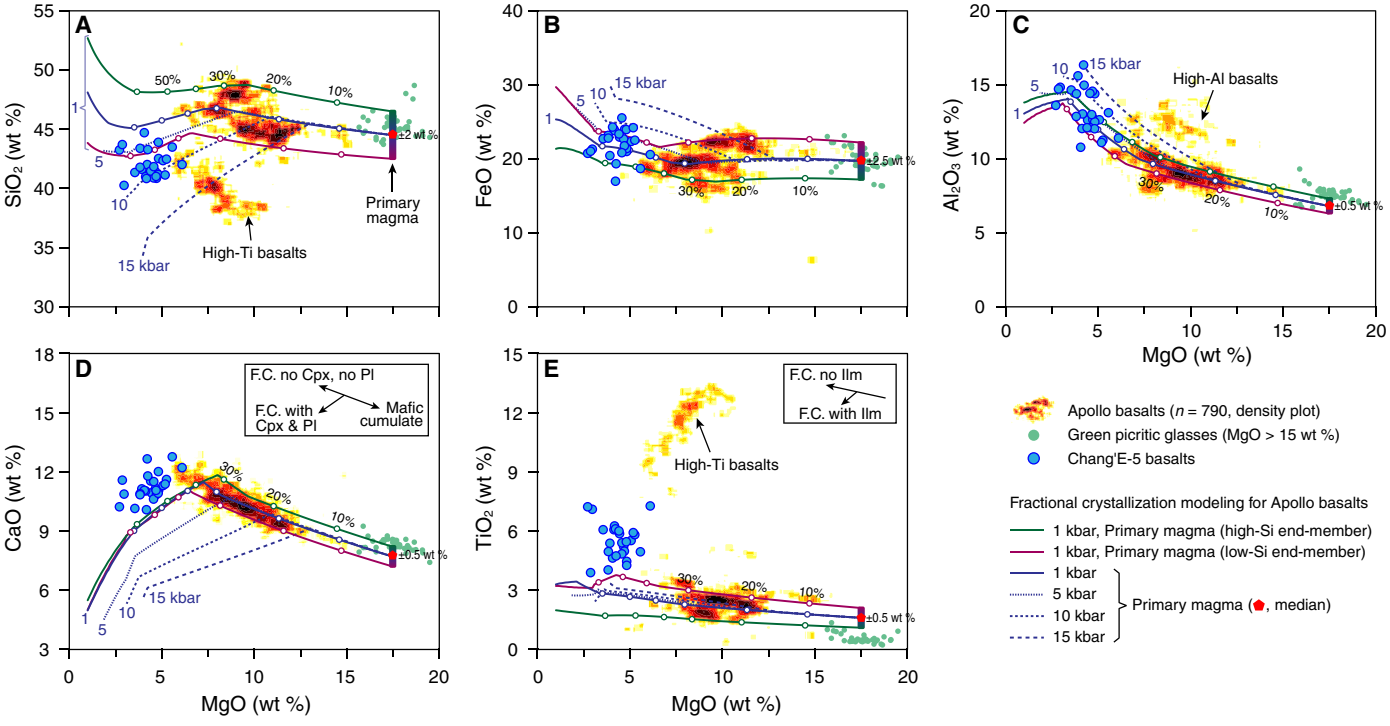

Fig. 1. Fractional crystallization modeling for Apollo basalts. (**A**) MgO versus SiO_2. (**B**) MgO versus FeO. (**C**) MgO versus Al_2O_3. (**D**) MgO versus CaO. (**E**) MgO versus TiO_2. The Apollo basalt data ($n = 790$) are from the ApolloBasaltDB_v2 database (*20*), which have been filtered to exclude KREEP-like (K, rare earth elements, and P) basalts. The Apollo basalts are shown on the basis of kernel density estimation. Green picritic glass (MgO > 15 wt %) data are from (*21*, *22*). Fractionation modeling was performed at constant pressures of 1, 5, 10, and 15 kbar for low-Ti basalts using the PETROLOG program. The crystallization sequence is olivine → clinopyroxene → plagioclase → ilmenite. To cover most Apollo samples, the starting compositions for primary magmas are extended across a large range (gradient color bar), including high-Si, median, and low-Si end-members. Compared to the CE5 basalts that experienced extensive fractionation, the Apollo basalts underwent low-degree, olivine-dominated fractionation. Primary magma compositions of the Apollo basalts are shown in table S2. Fractionation modeling results are given in data S1. Cpx, clinopyroxene; Pl, plagioclase; Ilm, ilmenite; F.C., fractional crystallization.

source hybridization, and mantle melting—to compare CE5 basalts with their Apollo counterparts.

Distinctive primary magma compositions

In the MgO versus Al_2O_3 plot (Fig. 1C), the CE5 and Apollo basalts broadly yield a potential fractional crystallization trend. This may suggest that they were derived from a similar primary magma. To test this idea, we carried out fractional crystallization modeling using the PETROLOG program (see Materials and Methods) (*23*). As Cr-spinel in the CE5 basalts appears as an early-stage crystallization phase (fig. S1G) and ilmenite represents a late-stage crystallization phase (fig. S2), these basalts cannot evolve from a high-Ti primary magma. Thus, the case of high-Ti magma crystallization can be excluded in our modeling. A starting composition close to picritic basalt 15387 (MgO = 17.4 wt % and TiO_2 = 1.67 wt %) (*24*) was used for preliminary modeling (red pentagon in Fig. 1 and table S2). This composition is at the high-MgO end of the Apollo basalts and falls within the range of green picritic glasses, making it a good candidate for the primary magma (as shown in fig. S3, assuming primary compositions with lower or higher MgO would not influence the fractionation trends). Our modeling at 1 kbar shows that olivine is a high-temperature liquidus phase, whereas clinopyroxene, plagioclase, and ilmenite crystallize at lower temperatures. The modeling reproduces the overall variations observed in the Apollo basalts, especially in terms of Al_2O_3 and CaO versus MgO (solid dark blue line in Fig. 1). The CaO contents increase steadily as MgO decreases, indicating that the Apollo basalts underwent olivine-dominated fractionation, consistent with previous studies (*6*, *16*). The Apollo basalts have variable SiO_2 and FeO contents, and thus, the starting compositions for the primary magma must be extended across a large range (Fig. 1 and table S2). The modeling trends (solid green and purple lines) span almost all compositions of Apollo basalts except for the high-Ti and the high-Al groups, which might result from assimilation (*25*, *26*). In contrast, the CE5 basalts deviate from these trends, with higher CaO and TiO_2, but lower SiO_2, contents. Even if high-pressure (5 to 15 kbar) fractional crystallization is considered, the CE5 basalts still exhibit higher CaO and TiO_2 contents than the deduced fractionation trends. Hence, it is likely that the CE5 and Apollo basalts were derived from different primary magmas.

To restore the primary magma compositions of the CE5 basalts, we used a reverse fractional crystallization method with the PETROLOG program (*23*). The principle is the addition of fractionated minerals back into the melt to move the melt composition up along the liquid line of descent toward more primitive composition. Mineral compositions used for the reverse modeling are determined through an iterative procedure with the PETROLOG program. The CE5 basalts show a roughly positive correlation ($r^2 = 0.26$) between CaO and MgO (Fig. 2D), indicating clinopyroxene as being part of the fractionating assemblage. Increasing Al_2O_3 with decreasing MgO implies that plagioclase was not a major fractionating

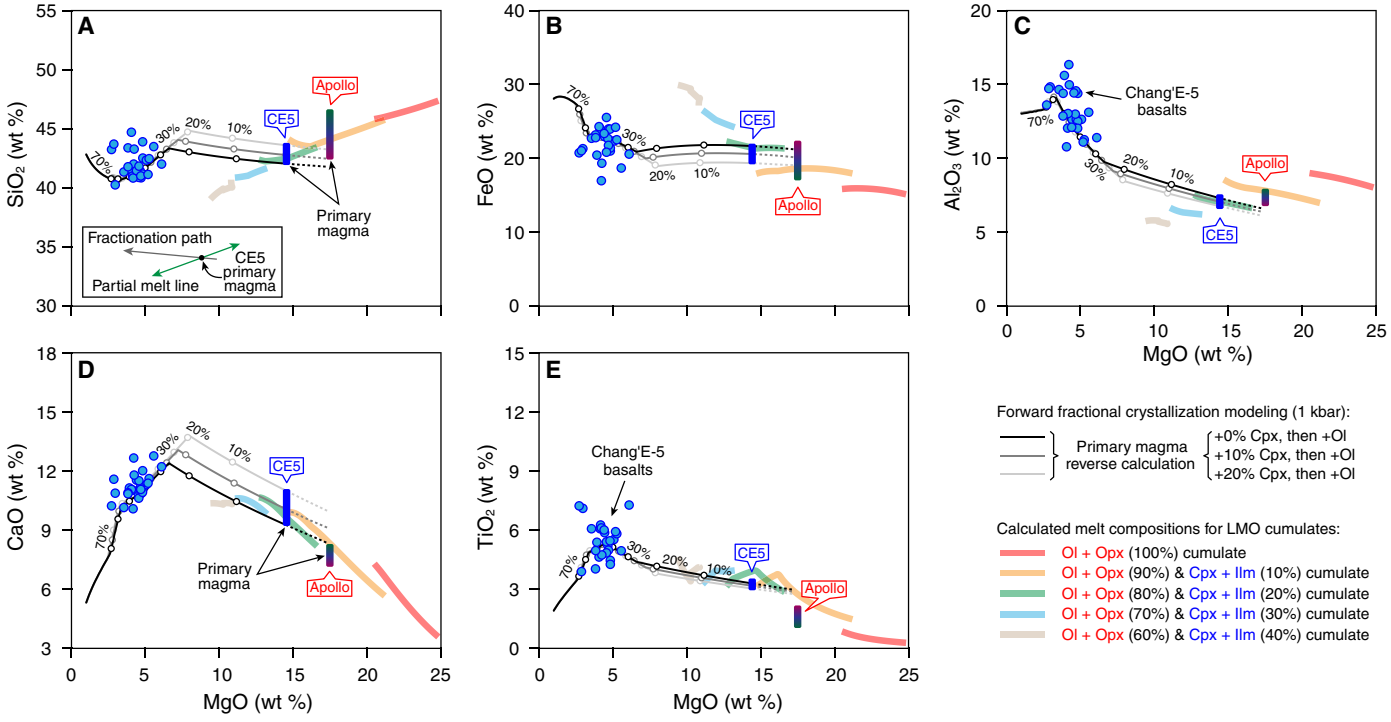

Fig. 2. Fractional crystallization modeling for CE5 basalts. (**A**) MgO versus SiO_2. (**B**) MgO versus FeO. (**C**) MgO versus Al_2O_3. (**D**) MgO versus CaO. (**E**) MgO versus TiO_2. Primary magma compositions of the CE5 basalts were reverse modeled with the addition of clinopyroxene (0, 10, and 20 mass %) and then olivine (excess) using the PETROLOG program at 1 kbar. Their specific compositions (blue bar; MgO = ~14 wt %) are defined by the intersection of the reverse fractionation paths and the partial melt trend lines (thick colored lines). Partial melt (F = 1 to 25 mol %) compositions of the hybrid mantle were calculated using the THERMOCALC program (see Fig. 3 for hybridization modeling). Primary magma compositions of the Apollo low-Ti basalts (gradient color bar) achieved in Fig. 1 are shown for comparison, which shows that the CE5 primary magma has higher CaO and TiO_2 than its Apollo counterparts. Fractionation modeling results and partial melt compositions are provided in data S2 and S3, respectively. Ol, olivine; Opx, orthopyroxene; other abbreviations are the same as Fig. 1.

phase (Fig. 2C), especially for MgO-rich samples. Thus, clinopyroxene was first added to the most MgO-enriched CE5 sample and then followed by olivine in the reverse fractionation modeling. It is uncertain how much clinopyroxene should be added before olivine appears. As a sensitivity test, we added 0, 10, or 20 mass % of clinopyroxene (Fig. 2). Although these options result in slightly different estimations for the primary magma compositions, they exert little influence on the fractionation trends for Mg-poor samples such as the CE5 basalts. Excess olivine was added in the reverse fractionation modeling, and the exact quantity will be constrained by mantle melting calculations (see the following section). Despite this semi-quantitative modeling here, the primitive compositions of CE5 basalts have higher CaO and TiO_2 contents than Apollo primary magmas (gradient color bar in Fig. 2). These primitive compositions may represent the primary magma or result from assimilation or crystal accumulation. Assimilation of subcrustal clinopyroxene-ilmenite cumulates could simultaneously elevate CaO and TiO_2 contents in the CE5 magmas. However, it would also substantially reduce their Al_2O_3 contents because of low Al_2O_3 contents (<3 wt %) of clinopyroxene-ilmenite cumulates (*27*), which is at odds with the data. Although accumulation of clinopyroxene, plagioclase, and ilmenite could explain the CE5 compositions, it requires nearly two-thirds of minerals in CE5 basalts to be an accumulation origin, which is highly unlikely because of the well-characterized basaltic textures (fig. S1). Moreover, in CE5 basalts, pyroxene is zoned with high-Ca cores and low-Ca rims (*12*), and olivine has higher Ti contents than the Apollo counterparts (*19*). All these indicate that the high CaO and TiO_2 contents are fingerprints of the CE5 primary magma.

Contributions of late-stage LMO cumulates to the CE5 mare source

There are two possibilities to account for the distinctive primary magma compositions of the CE5 and Apollo basalts: (i) They could share a common mantle source but originated from different depths, or (ii) they were derived from different mantle sources. Experimental simulations and thermodynamic calculations of mantle melting (*28*, *29*) demonstrate that the CaO content of the melt generally decreases with increasing pressure because of the increase in clinopyroxene modal abundance in the residue. It is ambiguous whether TiO_2 in melt tends to increase or decrease as pressure changes, but the TiO_2 content of the melt does not change notably with pressure (*29*). Moreover, our following calculations reveal the overlap of CE5 and Apollo basalt source depths. Therefore, the scenario of melting from a common source at different depths cannot be the first-order reason.

Alternatively, Apollo and CE5 mare melts originated from different mantle sources. The LMO cumulate stratigraphy consists of early formed ultramafic cumulates (mainly olivine and orthopyroxene) and late-stage clinopyroxene-ilmenite cumulates (*4*, *14*, *30*). The latter make up <10 volume percent (volume %) of the total cumulates. Previous studies suggest that the Apollo low-Ti basalts and green picritic glasses were multiply saturated with olivine-orthopyroxene

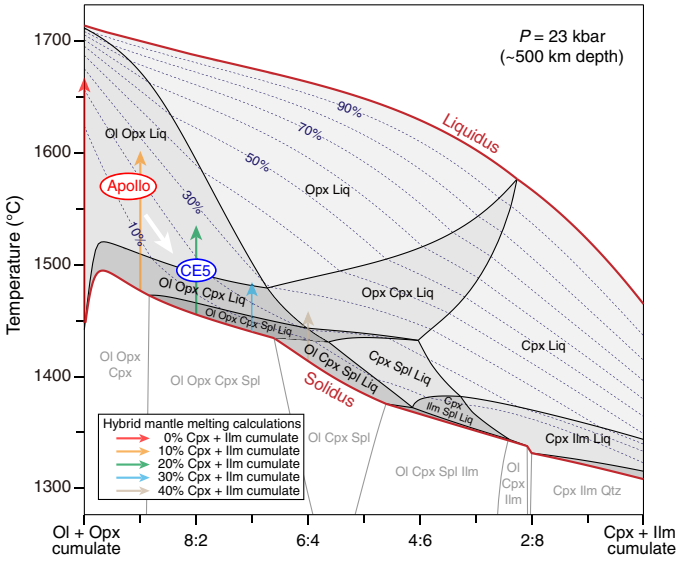

Fig. 3. A binary mixing model of LMO cumulate hybridization. Temperature-composition pseudosection was calculated using the THERMOCALC program at 23 kbar, corresponding to the average depth (~500 km) of basalt sources (Fig. 4). Compositions of the two end-member cumulates (Ol-Opx and Cpx-Ilm) are collected from (*30*) and given in table S2. The dashed lines show the non-modal batch melt proportion (as mole percent, ~volume percent). The vertical lines with arrows indicate melting trends with varying proportions of clinopyroxene-plagioclase cumulates in the hybrid mantle. The melting temperatures of Apollo and CE5 basalts were determined by the calculations of multiple saturation points (MSPs) (Fig. 4). Liq, liquid; Spl, spinel; Qtz, quartz; other abbreviations are the same as the previous figures.

residual sources (*31*, *32*), consistent with our phase equilibrium simulations using primary magma compositions (see below). Hence, the Apollo low-Ti basalts have a mantle source dominated by the early LMO cumulates. In contrast, the high CaO and TiO_2 contents of the CE5 primary magma (Fig. 2) instead suggest that clinopyroxene-ilmenite cumulates might have been involved in producing the young basalts. The late-stage cumulates are dense and could sink in the mantle and hybridize early, deep cumulates during mantle overturn (*5*, *14*, *15*). To test this hypothesis, we performed a binary mixing and non-modal melting simulation with the THERMOCALC program (see Materials and Methods) (*29*). The simulation shows that the mixing of olivine-orthopyroxene cumulates with clinopyroxene-ilmenite cumulates markedly reduces the melting temperature of the lunar mantle (Fig. 3). Partial melt compositions of hybrid sources have been calculated with adding 0, 10, 20, 30, and 40 mass % of clinopyroxene-ilmenite cumulate. As shown in Fig. 2, CaO and TiO_2 contents of the melts increase as source hybridization enhances. The intersection of partial melt trend lines and reverse fractionation paths defines the primary magma composition for the CE5 basalts (blue bar in Fig. 2 and table S2) and suggests the involvement of ~20 mass % of clinopyroxene-ilmenite cumulate in the CE5 source. These results indicate that the fusible late-stage LMO cumulates contributed much to the young CE5 basalt formation.

Young mare volcanism on the cooling Moon

The pressure and temperature (*P*-*T*) of multiple saturation points (MSPs) are commonly interpreted as the *P*-*T* condition at which magma segregated from its source (*6*, *7*, *32*). Thus, the *P*-*T* condition of MSP can be used to track the thermal state of the Moon. However, as mare basalts have undergone fractional crystallization and cannot represent their primary magmas, their MSP conditions are typically underestimated using the basalt bulk compositions. In this study, we have restored the primary magma compositions of Apollo and CE5 basalts. Their MSP conditions can be determined using phase equilibrium calculations with the THERMOCALC program (see Materials and Methods). All calculated liquidi are saturated with olivine at relatively low pressures and with orthopyroxene at high pressures. The intersection of the olivine-in and orthopyroxene-in curves defines the MSP (Fig. 4). The primary magmas of Apollo basalts have MSP at 1511° to 1576°C and 14.9 to 28.4 kbar, broadly consistent with those of picritic glasses (*31*, *33*, *34*). These conditions jointly imply a lunar mantle potential temperature of ~1440°C between 3.8 and 3.1 Ga ago. In contrast, the young CE5 magma has MSP at 1472° to 1496°C and 22.4 to 26.9 kbar, corresponding to a lunar mantle potential temperature of ~1360°C. These results demonstrate a sustained cooling (~80°C) history of the lunar mantle between 3.8 to 3.1 and 2.0 Ga ago.

The mechanism for generating young mare volcanism on the cooling Moon is an outstanding problem. Previous studies generally ascribed prolonged mare volcanism to the contributions from radiogenic heating (*9*, *35*) and/or mantle melting point depression due to enrichment in incompatible elements (*36*). However, Sm-Nd, Rb-Sr, and Pb isotopic data of the CE5 basalts consistently indicate that their mantle source region contained very few radiogenic and incompatible elements (*10*–*12*), implying that neither of the associated melting mechanisms produced these basalts. Moreover, a dry mantle source for the CE5 basalts excludes the possibility of hydrous mantle melting (*13*). Other hypotheses for prolonged lunar volcanism such as tidal heating (*37*), megaregolith insulation (*38*), and sluggish mantle convection (*39*) are possible but require further evidence. Our study shows that the young CE5 mantle source region had more clinopyroxene-ilmenite cumulates than those of older Apollo low-Ti basalts. The involvement of these fusible cumulates could lower the mantle melting point to offset the Moon's cooling (Fig. 3), absolving the need to invoke theoretical contributions from radiogenic and incompatible elements to trigger young lunar volcanism. Thus, the radiogenic heat-producing elements concentrated in the last dregs of the LMO melt must be decoupled from the late clinopyroxene-ilmenite cumulates, which suggests that the LMO cumulate overturn began to occur while solidification was active (*40*). Although the duration and scale of LMO cumulate overturn and mantle convective mixing remain poorly understood (*15*, *41*, *42*), it follows that the longer the time interval, the higher proportion of cumulate mixing and, thus, the lower the melting point. Therefore, mantle melting point depression by adding fusible components into the lunar upper mantle might be a viable mechanism for driving young mare volcanic activity on the Moon. The late fusible cumulates would sink to the lunar core-mantle boundary because of their high density (*42*, *43*). Thus, the addition of these components into the CE5 basalt source indicates that some late fusible domains stayed in the upper mantle (*40*, *44*) or rose into the upper mantle because of upwelling after overturn (*45*, *46*). The upward advection of fusible cumulates that had sunk during the LMO is consistent with convective overturn of the lunar mantle (*5*, *14*, *15*). This framework for delivering fusible cumulates to generate the CE5 basalts, thus, additionally implies that mantle convection continued to transfer internal heat into the shallow mantle via mantle upwelling as late as 2 Ga ago.

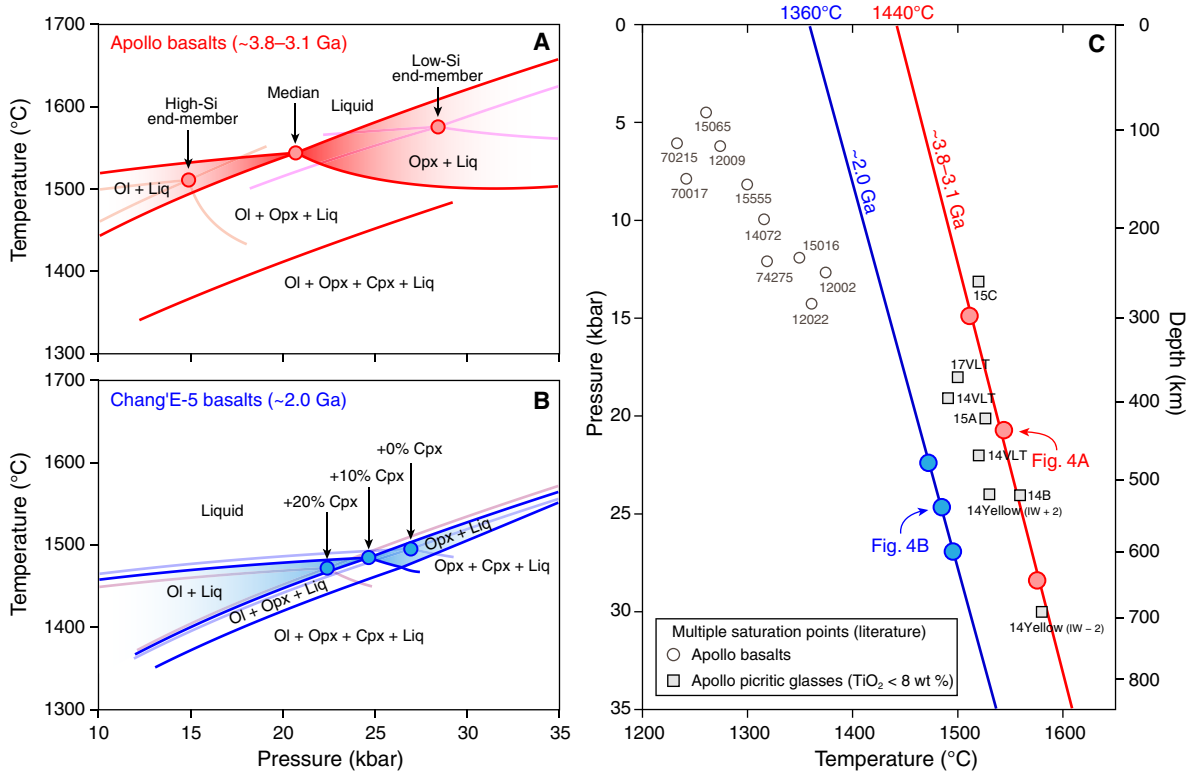

Fig. 4. Thermal evolution of the Moon inferred from MSP modeling. (**A**) Phase equilibrium calculations of the primary magmas of Apollo basalts illustrating their MSP *P-T* conditions (red circles). (**B**) Phase relation calculations of the primary magmas of CE5 basalts showing their MSP *P-T* conditions (blue circles). (**C**) *P-T* conditions inferred from the MSP of basalts and picritic glasses (TiO_2 < 8 wt %). Our calculations show that olivine is the liquidus phase until orthopyroxene joins and replaces it at high pressures. The pressures and temperatures at which primary magmas are multisaturated with these two phases define the MSP. The MSP *P-T* conditions of Apollo basalts (gray circles) and picritic glasses (gray squares) are compiled in (*33*, *34*). The red and blue lines correspond to the Moon's thermal profiles at 3.8 to 3.1 and 2.0 Ga ago, respectively, which show ~80°C cooling of the lunar mantle in >1 Ga. Mineral abbreviations are the same as the previous figures. IW, iron-wüstite buffer.

MATERIALS AND METHODS

Quantitative analysis of bulk compositions of CE5 basalt clasts

Twenty-seven representative basalt clasts were picked, mounted, polished, carbon-coated, and examined with the scanning electron microscope (SEM; Zeiss Gemini 450) at the Institute of Geology and Geophysics, Chinese Academy of Sciences in Beijing. Whole-rock major element compositions of lithic clasts are conventionally estimated on the basis of mineral average compositions, density, and modal abundances. Modal abundances are obtained through the point counting method. For the CE5 basalt clasts, however, chemical zoning in clinopyroxene and olivine is ubiquitous (fig. S4; mineral compositions are given in data S4), so the routine method may lead to large errors in the estimation of average mineral compositions. Thus, we use a quantitative x-ray mapping method with SEM energy-dispersive spectrometry (EDS; Oxford Instruments) to determine the bulk major element compositions of the CE5 basalt clasts, following the method in (*18*). The procedure includes x-ray map collection, raw count output (one for each element analysis), and background correction. The average compositions of pyroxene, olivine, and plagioclase are analyzed by the quantitative EDS mapping method (*18*). For those fine-grained, compositionally homogeneous minerals such as ilmenite, spinel, silica, K-feldspar, phosphates, and sulfides, we use EDS point analysis to acquire their average compositions, with 10 analyses for each phase. Mapping conditions are 20-kV accelerating voltage, 5-nA beam current, 8.5-mm working distance, and 200-μs collection time at each pixel. A total map collection time for each clast is ~40 min with a spatial resolution of ~500 nm. A set of certified reference materials (Micro-Analysis Consultants Ltd. Standards) was used to standardize the spectrometer: albite for Si, Na, and Al; diopside for Ca; olivine for Mg; almandine for Fe; $RbTiOPO_4$ for Ti; orthoclase for K; bustamite for Mn; and chromite for Cr. The detection limit of major elements is ~0.1 wt %. The precision and accuracy are better than 1 and 2%, respectively. The lunar meteorite NWA 4734 was used as a monitor sample; the integrated x-ray mapping composition of which matches well with the result obtained by inductively coupled plasma mass spectrometry (*47*). All void pixels were subtracted before bulk compositions were normalized to 100%. The average bulk chemistry obtained here is identical to the published data within error (table S1). Moreover, the average FeO (22.1 ± 1.9 wt %) and TiO_2 (5.5 ± 0.9 wt %) contents of the studied CE5 basalt clasts agree with the data obtained by the Lunar Prospector gamma-ray spectrometer (~22.4 wt % of FeO and ~4.5 wt % of TiO_2) (*48*), further demonstrating the reliability of our results.

Fractional crystallization modeling

Forward and reverse fractional crystallization processes were modeled using the PETROLOG program (*23*) to restore the primary magma compositions of the CE5 and Apollo basalts. All modeling

assumed pure fractional crystallization (100%) at a constant pressure. Fe_2O_3 in the melt was calculated using Fe^{3+} = 0 buffer of oxygen fugacity. Mineral solution models used here include olivine (*49*), clinopyroxene (*50*), orthopyroxene (*51*), plagioclase (*50*), and ilmenite (*52*). Spinel was excluded from our modeling because its abundance is very low (<1 volume %) in mare basalts, and available spinel solution models are unfit for fractionation modeling of the Ti-rich mare magmas. The pressure of near-surface fractionation was set at 1 kbar (corresponding to a depth of ~15 km) because the differences among the modeling results when pressures are less than 1 kbar are negligible. Modeling results at higher pressures (5, 10, and 15 kbar) are also given in Fig. 1 for reference. The detailed steps of reverse fractionation modeling are shown in the "Distinctive primary magma compositions" section of the body text. As shown in fig. S5, the calculated mineral compositions are in good agreement with the measured values of the CE5 basalts, verifying that our reverse fractionation modeling was done effectively. Primary magma compositions estimated in this work are presented in table S2.

LMO cumulate hybridization and mantle melting modeling

The mixing of early formed LMO cumulates with late-stage cumulates and the partial melting of these hybrid cumulates were modeled using the THERMOCALC 3.50 program (*29*) with the internally consistent thermodynamic dataset of (*53*) (update tc-ds634). The modeling was performed in a comprehensive system (K_2O-Na_2O-CaO-FeO-MgO-Al_2O_3-SiO_2-TiO_2-Cr_2O_3) using the recent thermodynamic models of orthopyroxene, olivine, clinopyroxene, ilmenite, spinel, and melt from (*29*). These new models have been proven to successfully reproduce the phase relations and melt compositions of ultramafic rocks (*29*). Therefore, they can well predict the melting conditions and melt compositions of the hybrid lunar mantle. The two end-member compositions of olivine-orthopyroxene and clinopyroxene-ilmenite cumulates used in Fig. 3 are collected from (*30*), in which they were calculated from the LMO with the lunar primitive upper mantle starting compositions (*54*). The cumulate composition data are provided in table S2. LMO cumulate hybridization and non-modal batch melting were modeled at 23 kbar, corresponding to the average depth (~500 km) of mare magma generation (Fig. 4C). Melt compositions shown in Fig. 2 represent 1 to 25 mole percent (mol %) degree of partial melting of the hybrid cumulates containing 0, 10, 20, 30, and 40 mass % of clinopyroxene-ilmenite cumulate.

MSP modeling

The pressure and temperature conditions of the MSP of CE5 and Apollo primary magmas were determined by phase equilibrium calculations with the THERMOCALC 3.50 program (*29*). The thermodynamic dataset and mineral models are the same as described earlier. Fe_2O_3 was set to zero, corresponding to oxygen fugacities below the iron-wüstite buffer. As primary magmas of the CE5 and Apollo basalts have quite low TiO_2 contents (~3 and 1.5 wt %, respectively), the effect of oxygen fugacity changes on our MSP simulations can be negligible (*33*). Near-liquidus phase relations were calculated from 10 to 35 kbar for a wide temperature range (Fig. 4). All calculated liquidi (i.e., the CE5 and Apollo primary magmas) are saturated with olivine at relatively low pressures and with orthopyroxene at high pressures. The intersection of the olivine-in and orthopyroxene-in curves defines the MSP. Although both the Apollo and CE5 primary magmas were multiply saturated with olivine and orthopyroxene, the MSP of the CE5 magma is closer to the clinopyroxene-in curve, implying more clinopyroxene in its source. The reliability of the modeled MSP results was evaluated by comparison with published experimental results. As shown in fig. S6, the calculated MSP conditions of lunar picritic glasses match well with those of experimental studies, demonstrating the reliability of our calculations.

SUPPLEMENTARY MATERIALS

Supplementary material for this article is available at https://science.org/doi/10.1126/sciadv.abn2103

REFERENCES AND NOTES

1. J. V. Smith, A. T. Anderson, R. C. Newton, E. J. Olsen, A. V. Crewe, M. S. Isaacson, D. Johnson, P. J. Wyllie, Petrologic history of the moon inferred from petrography, mineralogy and petrogenesis of Apollo 11 rocks, in *Proceedings of the Apollo 11 Lunar Science Conference* (Percammon Press, 1970), vol. 1, pp. 897–925.
2. J. A. Wood, J. S. Dickey Jr., U. B. Marvin, B. Powell, Lunar anorthosites and a geophysical model of the moon, in *Proceedings of the Apollo 11 Lunar Science Conference* (Percammon Press, 1970), vol. 1, pp. 965–988.
3. C. R. Neal, L. A. Taylor, Petrogenesis of mare basalts: A record of lunar volcanism. *Geochim. Cosmochim. Acta* **56**, 2177–2211 (1992).
4. C. K. Shearer, J. J. Papike, Magmatic evolution of the Moon. *Am. Mineral.* **84**, 1469–1494 (1999).
5. A. E. Ringwood, S. E. Kesson, A dynamic model for mare basalt petrogenesis, in *Proceedings of the 7th Lunar Science Conference* (Percammon Press, 1976), vol. 7, pp. 1697–1722.
6. J. Longhi, Experimental petrology and petrogenesis of mare volcanics. *Geochim. Cosmochim. Acta* **56**, 2235–2251 (1992).
7. S. M. Elardo, C. K. Shearer, K. E. Vander Kaaden, F. M. McCubbin, A. S. Bell, Petrogenesis of primitive and evolved basalts in a cooling Moon: Experimental constraints from the youngest known lunar magmas. *Earth Planet. Sci. Lett.* **422**, 126–137 (2015).
8. J. F. Snape, A. A. Nemchin, M. J. Whitehouse, R. E. Merle, T. Hopkinson, M. Anand, The timing of basaltic volcanism at the Apollo landing sites. *Geochim. Cosmochim. Acta* **266**, 29–53 (2019).
9. L. E. Borg, C. K. Shearer, Y. Asmerom, J. J. Papike, Prolonged KREEP magmatism on the Moon indicated by the youngest dated lunar igneous rock. *Nature* **432**, 209–211 (2004).
10. X. C. Che, A. Nemchin, D. Y. Liu, T. Long, C. Wang, M. D. Norman, K. H. Joy, R. Tartèse, J. Head, B. Jolliff, J. F. Snape, C. R. Neal, M. J. Whitehouse, C. Crow, G. Benedix, F. Jourdan, Z. Q. Yang, C. Yang, J. H. Liu, S. W. Xie, Z. M. Bao, R. L. Fan, D. P. Li, Z. S. Li, S. G. Webb, Age and composition of young basalts on the Moon, measured from samples returned by Chang'e-5. *Science* **374**, 887–890 (2021).
11. Q. L. Li, Q. Zhou, Y. Liu, Z. Y. Xiao, Y. T. Lin, J. H. Li, H. X. Ma, G. Q. Tang, S. Guo, X. Tang, J. Y. Yuan, J. Li, F. Y. Wu, Z. Y. Ouyang, C. L. Li, X. H. Li, Two-billion-year-old volcanism on the Moon from Chang'E-5 basalts. *Nature* **600**, 54–58 (2021).
12. H. C. Tian, H. Wang, Y. Chen, W. Yang, Q. Zhou, C. Zhang, H. L. Lin, C. Huang, S. T. Wu, L. H. Jia, L. Xu, D. Zhang, X. G. Li, R. Chang, Y. H. Yang, L. W. Xie, D. P. Zhang, G. L. Zhang, S. H. Yang, F. Y. Wu, Non-KREEP origin for Chang'E-5 basalts in the Procellarum KREEP Terrane. *Nature* **600**, 59–63 (2021).
13. S. Hu, H. C. He, J. L. Ji, Y. T. Lin, H. J. Hui, M. Anand, R. Tartèse, Y. H. Yan, J. L. Hao, R. Y. Li, L. X. Gu, Q. Guo, H. Y. He, Z. Y. Ouyang, A dry lunar mantle reservoir for young mare basalts of Chang'e-5. *Nature* **600**, 49–53 (2021).
14. G. A. Snyder, L. A. Taylor, C. R. Neal, A chemical model for generating the sources of mare basalts: Combined equilibrium and fractional crystallization of the lunar magmasphere. *Geochim. Cosmochim. Acta* **56**, 3809–3823 (1992).
15. L. T. Elkins-Tanton, S. Burgess, Q. Z. Yin, The lunar magma ocean: Reconciling the solidification process with lunar petrology and geochronology. *Earth Planet. Sci. Lett.* **304**, 326–336 (2011).
16. J. J. Papike, F. N. Hodges, A. E. Bence, M. Cameron, J. M. Rhodes, Mare basalts: Crystal chemistry, mineralogy, and petrology. *Rev. Geophys. Space Phys.* **14**, 475–540 (1976).
17. C. L. Li, H. Hu, M. F. Yang, Z. Y. Pei, Q. Zhou, X. Ren, B. Liu, D. W. Liu, X. G. Zeng, G. L. Zhang, H. B. Zhang, J. J. Liu, Q. Wang, X. J. Deng, C. J. Xiao, Y. G. Yao, D. S. Xue, W. Zuo, Y. Sun, W. B. Wen, Z. Y. Ouyang, Characteristics of the lunar samples returned by Chang'E–5 mission. *Natl. Sci. Rev.* **9**, nwab188 (2022).
18. J. Yuan, Y. Chen, D. Zhang, X. Li, H. Tian, W. Yang, W. Su, Quantitative analysis of bulk composition of small-size lunar samples using energy dispersive X-ray spectroscopy. *At. Spectrosc.* **43**, 292–302 (2022).
19. D. Zhang, B. Su, Y. Chen, W. Yang, Q. Mao, L. H. Jia, Titanium in olivine reveals low-Ti origin of the Chang'E-5 lunar basalts. *Lithos* **414**, 106639 (2022).

20. K. A. Cone, ApolloBasalt DB_V2, version 1.0 (Interdisciplinary Earth Data Alliance, 2021).
21. J. W. Delano, Pristine lunar glasses: Criteria, data, and implications. *J. Geophys. Res. Solid Earth* **91**, 201–213 (1986).
22. C. K. Shearer, J. J. Papike, Basaltic magmatism on the Moon: A perspective from volcanic picritic glass beads. *Geochim. Cosmochim. Acta* **57**, 4785–4812 (1993).
23. L. V. Danyushevsky, P. Plechov, Petrolog3: Integrated software for modeling crystallization processes. *Geochem. Geophys. Geosyst.* **12**, Q07021 (2011).
24. G. Ryder, A. Steele, Chemical dispersion among Apollo 15 olivine-normative mare basalts, in *Proceedings of the 18th Lunar and Planetary Science Conference* (Lunar and Planetary Institute, 1988), pp. 273–282.
25. N. J. Hubbard, J. W. Minear, A physical and chemical model of early lunar history, in *Proceedings of the 6th Lunar Science Conference* (Percammon Press, 1975), pp. 1057–1085.
26. H. J. Hui, C. R. Neal, C. Y. Shih, L. E. Nyquist, Petrogenetic association of the oldest lunar basalts: Combined Rb–Sr isotopic and trace element constraints. *Earth Planet. Sci. Lett.* **373**, 150–159 (2013).
27. Y. Lin, E. J. Tronche, E. S. Steenstra, W. van Westrenen, Experimental constraints on the solidification of a nominally dry lunar magma ocean. *Earth Planet. Sci. Lett.* **471**, 104–116 (2017).
28. M. J. Walter, Melting of garnet peridotite and the origin of komatiite and depleted lithosphere. *J. Petrol.* **39**, 29–60 (1998).
29. E. L. Tomlinson, T. J. Holland, A thermodynamic model for the subsolidus evolution and melting of peridotite. *J. Petrol.* **62**, egab012 (2021).
30. T. E. Johnson, L. J. Morrissey, A. A. Nemchin, N. J. Gardiner, J. F. Snape, The phases of the Moon: Modelling crystallisation of the lunar magma ocean through equilibrium thermodynamics. *Earth Planet. Sci. Lett.* **556**, 116721 (2021).
31. L. T. Elkins, V. A. Fernandes, J. W. Delano, T. L. Grove, Origin of lunar ultramafic green glasses: Constraints from phase equilibrium studies. *Geochim. Cosmochim. Acta* **64**, 2339–2350 (2000).
32. T. L. Grove, M. J. Krawczynski, Lunar mare volcanism: Where did the magmas come from? *Elements* **5**, 29–34 (2009).
33. S. M. Brown, T. L. Grove, Origin of the Apollo 14, 15, and 17 yellow ultramafic glasses by mixing of deep cumulate remelts. *Geochim. Cosmochim. Acta* **171**, 201–215 (2015).
34. L. T. Elkins-Tanton, B. H. Hager, T. L. Grove, Magmatic effects of the lunar late heavy bombardment. *Earth Planet. Sci. Lett.* **222**, 17–27 (2004).
35. M. A. Wieczorek, R. J. Phillips, The "Procellarum KREEP Terrane": Implications for mare volcanism and lunar evolution. *J. Geophys. Res. Planets* **105**, 20417–20430 (2000).
36. S. M. Elardo, M. Laneuville, F. M. McCubbin, C. K. Shearer, Early crust building enhanced on the Moon's nearside by mantle melting-point depression. *Nat. Geosci.* **13**, 339–343 (2020).
37. Y. Harada, S. Goossens, K. Matsumoto, J. Yan, J. Ping, H. Noda, J. Haruyama, Strong tidal heating in an ultralow-viscosity zone at the core–mantle boundary of the Moon. *Nat. Geosci.* **7**, 569–572 (2014).
38. R. Ziethe, K. Seiferlin, H. Hiesinger, Duration and extent of lunar volcanism: Comparison of 3D convection models to mare basalt ages. *Planetary Space Sci.* **57**, 784–796 (2009).
39. R. N. Mitchell, Chang'E-5 reveals the Moon's secrets to a longer life. *The Innovation* **2**, 100177 (2021).
40. Y. Zhao, J. De Vries, A. van den Berg, M. Jacobs, W. van Westrenen, The participation of ilmenite-bearing cumulates in lunar mantle overturn. *Earth Planet. Sci. Lett.* **511**, 1–11 (2019).
41. N. Dygert, G. Hirth, Y. Liang, A flow law for ilmenite in dislocation creep: Implications for lunar cumulate mantle overturn. *Geophys. Res. Lett.* **43**, 532–540 (2016).
42. N. Zhang, E. Parmentier, Y. Liang, A 3-D numerical study of the thermal evolution of the Moon after cumulate mantle overturn: The importance of rheology and core solidification. *J. Geophys. Res. Planets* **118**, 1789–1804 (2013).
43. N. Zhang, N. Dygert, Y. Liang, E. Parmentier, The effect of ilmenite viscosity on the dynamics and evolution of an overturned lunar cumulate mantle. *Geophys. Res. Lett.* **44**, 6543–6552 (2017).
44. S. Kato, T. Morota, Y. Yamaguchi, S.-i. Watanabe, H. Otake, M. Ohtake, Magma source transition of lunar mare volcanism at 2.3 Ga. *Meteorit. Planet. Sci.* **52**, 1899–1915 (2017).
45. L. Tokle, G. Hirth, Y. Liang, P. Raterron, N. Dygert, The effect of pressure and Mg-content on ilmenite rheology: Implications for lunar cumulate mantle overturn. *J. Geophys. Res. Planets* **126**, e2020JE006494 (2021).
46. S. Zhong, E. Parmentier, M. T. Zuber, A dynamic origin for the global asymmetry of lunar mare basalts. *Earth Planet. Sci. Lett.* **177**, 131–140 (2000).
47. J. Chen, B. L. Jolliff, A. Wang, R. L. Korotev, K. Wang, P. K. Carpenter, H. Chen, Z. Ling, X. Fu, Y. Ni, Petrogenesis and shock metamorphism of basaltic lunar meteorites Northwest Africa 4734 and 10597. *J. Geophys. Res. Planets* **124**, 2583–2598 (2019).
48. T. H. Prettyman, J. J. Hagerty, R. C. Elphic, W. C. Feldman, D. J. Lawrence, G. W. McKinney, D. T. Vaniman, Elemental composition of the lunar surface: Analysis of gamma ray spectroscopy data from Lunar Prospector. *J. Geophys. Res. Planets* **111**, E12007 (2006).
49. C. E. Ford, D. G. Russell, J. A. Groven, M. R. Fisk, Olivine-liquid equilibria: Temperature, pressure and composition dependence of the crystal/liquid cation partition coefficients for Mg, Fe^{2+}, Ca and Mn. *J. Petrol.* **24**, 256–266 (1983).
50. L. V. Danyushevsky, The effect of small amounts of H_2O on crystallisation of mid-ocean ridge and backarc basin magmas. *J. Volcanol. Geotherm. Res.* **110**, 265–280 (2001).
51. P. Beattie, Olivine–melt and orthopyroxene–melt equilibria. *Contrib. Mineral. Petrol.* **115**, 103–111 (1993).
52. R. L. Nielsen, EQUIL: A program for the modeling of low-pressure differentiation processes in natural mafic magma bodies. *Comput. Geosci.* **11**, 531–546 (1985).
53. T. J. B. Holland, R. Powell, An improved and extended internally consistent thermodynamic dataset for phases of petrological interest, involving a new equation of state for solids. *J. Metam. Geol.* **29**, 333–383 (2011).
54. J. Longhi, Petrogenesis of picritic mare magmas: Constraints on the extent of early lunar differentiation. *Geochim. Cosmochim. Acta* **70**, 5919–5934 (2006).

Acknowledgments: We are grateful to the China National Space Administration (CNSA) for providing the CE5 samples. We thank Y.-T. Lin, Q.-L. Li, and Q. Zhou for helpful discussions, Y.-B. Li for assistance with modeling, and C. Sun for logistical support. This paper benefited from constructive reviews by R. M. Palin, an anonymous reviewer, and the associate editor R. Klima. **Funding:** This work was supported by the Key Research Program of the Chinese Academy of Sciences (ZDBS-SSW-JSC007-15) and the Key Research Program of the Institute of Geology and Geophysics, Chinese Academy of Sciences (IGGCAS-202101). **Author contributions:** Y.C. and B.S. conceived this study. H.T. and W.Y. prepared the samples. J.Y. conducted the experimental analyses. B.S. performed the modeling. R.N.M., W.Y., H.H., H.W., X.-H.L., and F.-Y.W. contributed to data interpretation. B.S. and Y.C. wrote the manuscript with input from all authors. **Competing interests:** The authors declare that they have no competing interests. **Data and materials availability:** The analytical data and detailed results of fractional crystallization and mantle melting simulations are available in the Supplementary Materials. The code used to calculate the hybrid cumulate mantle and MSPs is readily available at the THERMOCALC website, at https://hpxeosandthermocalc.org/.

Submitted 11 November 2021
Accepted 8 September 2022
Published 21 October 2022
10.1126/sciadv.abn2103